February 2, 2008 15:46 WSPC - Proceedings Trim Size: 9in x 6in   romerogomez

The formation of spiral arms and rings in barred galaxies

M. Romero-Gómez* and E. Athanassoula

Laboratoire d'Astrophysique de Marseille,
Observatoire Astronomique de Marseille Provence,
2 Place Le Verrier 13248 Marseille, France
∗E-mail: merce.romerogomez@oamp.fr

J.J. Masdemont

I.E.E.C & Dep. Mat. Aplicada I, Universitat Politècnica de Catalunya,
Av. Diagonal 647, 08028 Barcelona, Spain

C. García-Gómez

D.E.I.M., Universitat Rovira i Virgili,
Av. Països Catalans 26, 43007 Tarragona, Spain

We propose a new theory to explain the formation of spiral arms and of all types of outer rings in barred galaxies. We have extended and applied the technique used in celestial mechanics to compute transfer orbits. Thus, our theory is based on the chaotic orbital motion driven by the invariant manifolds associated to the periodic orbits around the hyperbolic equilibrium points. In particular, spiral arms and outer rings are related to the presence of heteroclinic or homoclinic orbits. Thus, R_1 rings are associated to the presence of heteroclinic orbits, while $R_1 R_2$ rings are associated to the presence of homoclinic orbits. Spiral arms and R_2 rings, however, appear when there exist neither heteroclinic nor homoclinic orbits. We examine the parameter space of three realistic, yet simple, barred galaxy models and discuss the formation of the different morphologies according to the properties of the galaxy model. The different morphologies arise from differences in the dynamical parameters of the galaxy.

Keywords: galactic dynamics - invariant manifolds - spiral structure - ring structure

1. Introduction

Bars are very common features in disk galaxies. According to Eskridge *et al.* [1] in the near infrared 56% of the galaxies are strongly barred and 6% are weakly barred. A large fraction of barred galaxies show either spiral

2

arms emanating from the ends of the bar or spirals that end up forming outer rings (Elmegreen & Elmegreen [2]; Sandage & Bedke [3]).

Spiral arms are believed to be density waves (Lindblad [4]). Toomre [5], finds that the spiral arms are density waves that propagate outwards towards the principal Lindblad resonances, where they damp. So other mechanisms for replenishment are needed (see for example Lindblad [6]; Toomre [5,9]; Toomre & Toomre [7]; Sanders & Huntley [8]; Athanassoula [10] for more details). Rings have been studied by Schwarz [11–13]. The author studies the response of a gaseous disk galaxy to a bar-like perturbation. He relates the rings with the position of the principal Lindblad resonances. There are different types of outer rings and they can be classified according to the relative orientation of the principal axes of the inner and outer rings (Buta [14]). If the two axes are perpendicular, the outer ring has an eight-shape and it is called R_1 ring. If they are parallel, it is called R_2 ring. There are galaxies where both types of rings are present, in which case the outer ring is simply called R_1R_2 ring.

Our approach is from the dynamical systems point of view. We first note that both spiral arms and (inner and outer) rings emanate from, or are linked to, the ends of the bar, where the unstable equilibrium points of a rotating system are located. We also note that, so far, no common theory for the formation of both features has been presented. We therefore study in detail the neighbourhood of the unstable points and we find that spiral arms and rings are flux tubes driven by the invariant manifolds associated to the periodic orbits around the unstable equilibrium points.

This paper is organised as follows. In Sec. 2, we give the characteristics of each component of the model and the potential used to describe it. In Sec. 3, we give the equations of motion and we study the neighbourhood of the equilibrium points. In particular, we give definitions of the Lyapunov periodic orbits, the invariant manifolds associated to them, and of the homoclinic and heteroclinic orbits. In Sec. 4, we present our results and in Sec. 5, we briefly summarise.

2. Description of the model

We use a model introduced in Athanassoula [15] that consists of the superposition of an axisymmetric and a bar-like component. The axisymmetric component is the superposition of a disc and a spheroid. The disc is modelled as a Kuzmin-Toomre disc (Kuzmin [16]; Toomre [17]) of surface

density $\Sigma(r)$ (see also left panel of Fig. 1):

$$\Sigma(r) = \frac{V_d^2}{2\pi r_d}\left(1 + \frac{r^2}{r_d^2}\right)^{-3/2}, \tag{1}$$

where the parameters V_d and r_d set the scales of the velocities and radii of the disc, respectively. The spheroid is modelled using a spherical density distribution, $\rho(r)$ (Eq. 2), characteristic for spheroids. In the middle panel of Fig.1, we plot the isodensity curves for this density function:

$$\rho(r) = \rho_b\left(1 + \frac{r^2}{r_b^2}\right)^{-3/2}, \tag{2}$$

where ρ_b and r_b determine the central density and scale-length of the spheroid.

Bars are non-axisymmetric features with high ellipticities. We will use three different bar models.In the first one the bar potential is described by a Ferrers ellipsoid (Ferrers [18]) whose density distribution is:

$$\rho_B(x,y) = \begin{cases} \rho_0(1-m^2)^n & m \leq 1 \\ 0 & m \geq 1, \end{cases} \tag{3}$$

where $m^2 = x^2/a^2 + y^2/b^2$. The values of a and b determine the shape of the bar, a being the length of the semi-major axis, which is placed along the x coordinate axis, and b being the length of the semi-minor axis. The parameter n measures the degree of concentration of the bar and ρ_0 represents the bar central density. In the right panel of Fig. 1, we plot the density function along the semi-major and semi-minor axes of the Ferrers ellipsoid with index $n = 2$, and principal axes $a = 6$ and $b = 1.5$.

We also use two ad-hoc potentials, namely a Dehnen's bar type (Dehnen [19]) and a Barbanis-Woltjer (BW) bar type (Barbanis & Woltjer [20]) to compare to the results obtained with the Ferrers ellipsoid. The Dehnen's bar potential has the following expression:

$$\Phi_1(r,\theta) = -\frac{1}{2}\epsilon v_0^2 \cos(2\theta)\begin{cases} 2 - \left(\dfrac{r}{\alpha}\right)^n, \ r \leq \alpha \\ \left(\dfrac{\alpha}{r}\right)^n, \qquad r \geq \alpha, \end{cases} \tag{4}$$

where the parameter α is a characteristic length scale and v_0 is a characteristic circular velocity. The parameter ϵ is related to the bar strength. The BW potential has the expression:

$$\Phi_2(r,\theta) = \hat{\epsilon}\sqrt{r}(r_1 - r)\cos(2\theta), \tag{5}$$

4

where the parameter r_1 is a characteristic scale length and $\hat{\epsilon}$ is related to the bar strength.
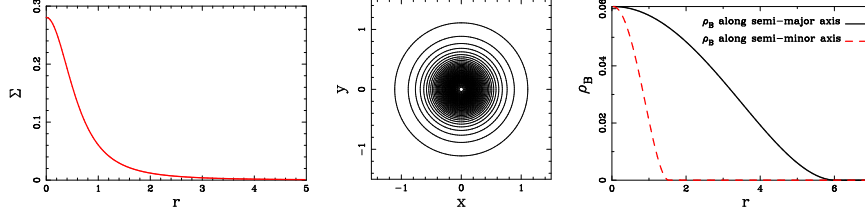

Fig. 1.   Characteristics of the components. *Left panel:* Density function of the Kuzmin-Toomre disc (red solid line) with $r_d = 0.75$ and $V_d = 1.5$. *Middle panel:* Isodensity curves for the spherical distribution representing the spheroid with parameters $r_b = 0.3326$ and $\rho_b = 23552.37$. *Right panel:* Density along the semi-major axis (black solid line) and the semi-minor axis (red dashed line) of a Ferrers bar with $n = 2$, $a = 6$, $b = 1.5$ and $\rho_0 = 0.0193$.

The bar-like component rotates anti-clockwise with angular velocity $\mathbf{\Omega_p} = \Omega_p \mathbf{z}$, where Ω_p is a constant pattern speed [a].

3. Equations of motion and dynamics around L_1 and L_2

The equations of motion in a frame rotating with angular speed $\mathbf{\Omega_p}$ in vector form are

$$\ddot{\mathbf{r}} = -\nabla\mathbf{\Phi} - 2(\mathbf{\Omega_p} \times \dot{\mathbf{r}}) - \mathbf{\Omega_p} \times (\mathbf{\Omega_p} \times \mathbf{r}), \qquad (6)$$

where the terms $-2\mathbf{\Omega_p} \times \dot{\mathbf{r}}$ and $-\mathbf{\Omega_p} \times (\mathbf{\Omega_p} \times \mathbf{r})$ represent the Coriolis and the centrifugal forces, respectively, Φ is the potential and $\mathbf{r}$ is the position vector. We define an effective potential $\Phi_{\text{eff}} = \Phi - \frac{1}{2}\Omega_p^2 (x^2 + y^2)$, then Eq. (6) becomes $\ddot{\mathbf{r}} = -\nabla\mathbf{\Phi}_{\text{eff}} - 2(\mathbf{\Omega_p} \times \dot{\mathbf{r}})$, and the Jacobi constant is

$$E_J = \frac{1}{2}|\dot{\mathbf{r}}|^2 + \Phi_{\text{eff}}, \qquad (7)$$

which, being constant in time, can be considered as the energy in the rotating frame. The surface $\Phi_{\text{eff}} = E_J$ (E_J defined as in Eq. (7)) is called the zero velocity surface, and its intersection with the $z = 0$ plane gives the zero velocity curve. All regions in which $\Phi_{\text{eff}} > E_J$ are forbidden to a star with this energy, and are thus called forbidden regions.

For our calculations we place ourselves in a frame of reference corotating with the bar, and the bar semi-major axis is located along the x axis. In this

---

[a]Bold letters denote vector notation. The vector $\mathbf{z}$ is a unit vector.

rotating frame we have five equilibrium points, which, due to the similarity with the Restricted Three Body Problem, are also called Lagrangian points (see left panel of Fig. 2). The points located symmetrically along the x axis, namely L_1 and L_2, are linearly unstable. The ones located on the origin of coordinates, namely L_3, and along the y axis, namely L_4 and L_5, are linearly stable. The zero velocity curve defines two different regions, namely, an exterior region and an interior one that contains the bar. The interior and exterior regions are connected via the equilibrium points (see middle panel of Fig. 2). Around the equilibrium points there exist families of periodic orbits, e.g. around the central equilibrium point the well-known x_1 family of periodic orbits that is responsible for the bar structure.

The dynamics around the unstable equilibrium points is described in detail in Romero-Gómez *et al.* [21]; here we give only a brief summary. Around each unstable equilibrium point there exists a family of periodic orbits, known as the family of Lyapunov orbits (Lyapunov [22]). For a given energy level, two stable and two unstable sets of asymptotic orbits emanate from the corresponding periodic orbit, and they are known as the stable and the unstable invariant manifolds, respectively. The stable invariant manifold is the set of orbits that tends to the periodic orbit asymptotically. In the same way, the unstable invariant manifold is the set of orbits that departs asymptotically from the periodic orbit (i.e. orbits that tend to the Lyapunov orbits when the time tends to minus infinity), as seen in the right panel of Fig. 2. Since the invariant manifolds extend well beyond the neighbourhood of the equilibrium points, they can be responsible for global structures.

In Romero-Gómez *et al.* [23], we give a detailed description of the role invariant manifolds play in global structures and, in particular, in the transfer of matter. Simply speaking, the transfer of matter is characterised by the presence of homoclinic, heteroclinic, and transit orbits.

Homoclinic orbits correspond to asymptotic trajectories that depart from the unstable Lyapunov periodic orbit γ around L_i and return asymptotically to it (see Fig. 3a). Heteroclinic orbits are asymptotic trajectories that depart from the periodic orbit γ around L_i and asymptotically approach the corresponding Lyapunov periodic orbit with the same energy around the Lagrangian point at the opposite end of the bar L_j, $i \neq j$ (see Fig. 3b). There also exist trajectories that spiral out from the region of the unstable periodic orbit, and we refer to them as transit orbits (see Fig. 3c). These three types of orbits are chaotic orbits since they fill part of the chaotic sea when we plot the Poincaré surface of section (e.g. the section $(x, \dot{x})$ near L_1).
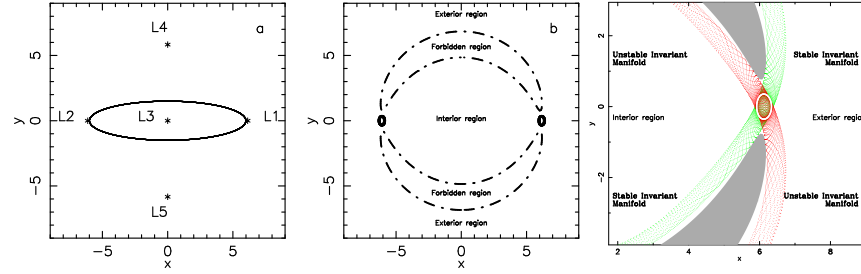
6

Fig. 2.   Dynamics around the L_1 and L_2 equilibrium points. *Left panel:* Position of the equilibrium points and outline of the bar. *Middle panel:* Zero velocity curves and Lyapunov periodic orbits around L_1 and L_2. *Right panel:* Unstable (in red) and stable (in green) invariant manifolds associated to the periodic orbit around L_1. In grey, we plot the forbidden region. From Romero-Gómez *et al.* 2006, Astronomy & Astrophysics, 453, 39, EDP Sciences.
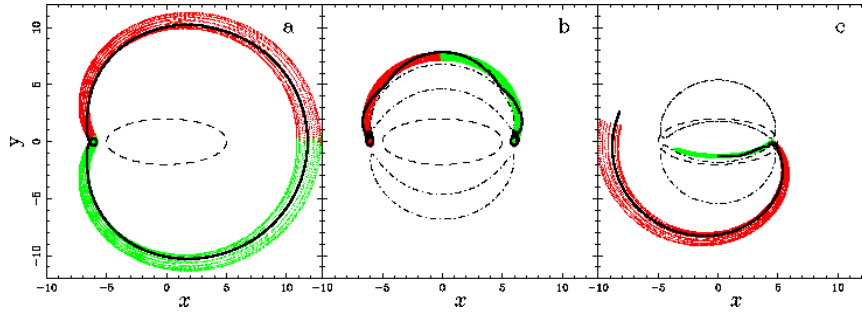

Fig. 3.   Homoclinic **(a)**, heteroclinic **(b)** and transit **(c)** orbits (black thick lines) in the configuration space. In red lines, we plot the unstable invariant manifolds associated to the periodic orbits, while in green we plot the corresponding stable invariant manifolds. In dashed lines, we give the outline of the bar and, in **(b)** and **(c)**, we plot the zero velocity curves in dot-dashed lines. From Romero-Gómez *et al.* 2007, Astronomy and Astrophysics, 472, 63, EDP Sciences.

4. Results

Here we describe the main results obtained when we vary the parameters of the models introduced in Sec. 2. One of our goals is to check separately the influence of each of the main free parameters. In order to do so, we make families of models in which only one of the free parameters is varied, while the others are kept fixed. Our results show that only the bar pattern speed and the bar strength have an influence on the shape of the invariant

manifolds, and thus, on the morphology of the galaxy (Romero-Gómez *et al.* [23]).

Our results also show that the morphologies obtained do not depend on the type of bar potential we use, but on the presence of homoclinic or heteroclinic orbits. If heteroclinic orbits exist, then the ring of the galaxy is classified as rR_1 (see Fig. 4a). The inner branches of the invariant manifolds associated to γ_1 and γ_2 outline an inner ring that encircles the bar and is elongated along it. The outer branches of the same invariant manifolds form an outer ring whose principal axis is perpendicular to the bar major axis. If the model does not have either heteroclinic or homoclinic orbits and only transit orbits are present, the barred galaxy will present two spiral arms emanating from the ends of the bar. The outer branches of the unstable invariant manifolds will spiral out from the ends of the bar and they will not return to its vicinity (see Fig. 4d). If the outer branches of the unstable invariant manifolds intersect in configuration space with each other, then they form the characteristic shape of R_2 rings (see Fig. 4b). That is, the trajectories outline an outer ring whose principal axis is parallel to the bar major axis. The last possibility is if only homoclinic orbits exist. In this case, the inner branches of the invariant manifolds for an inner ring, while the outer branches outline both types of outer rings, thus the barred galaxy presents an R_1R_2 ring morphology (see Fig. 4c).
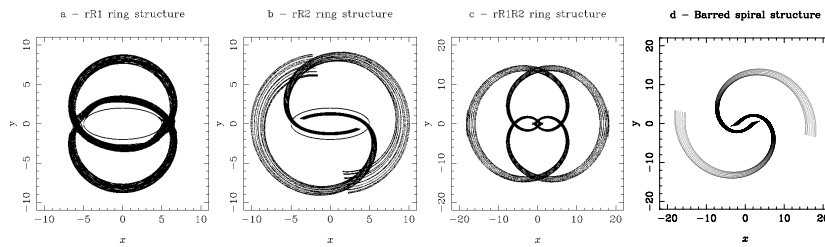

Fig. 4.   Rings and spiral arms structures. We plot the invariant manifolds for different models. **(a)** rR_1 ring structure. **(b)** rR_2 ring structure. **(c)** R_1R_2 ring structure. **(d)** Barred spiral galaxy. From Romero-Gómez *et al.* 2007, Astronomy and Astrophysics, 472, 63, EDP Sciences.

5. Summary

To summarise, our results show that invariant manifolds describe well the loci of the different types of rings and spiral arms. They are formed by

8

a bundle of trajectories linked to the unstable regions around the L_1/L_2 equilibrium points. The study of the influence of one model parameter on the shape of the invariant manifolds in the outer parts of the galaxy reveals that only the pattern speed and the bar strength affect the galaxy morphology. The study also shows that all the different ring types and spirals can be obtained when we vary the model parameters.

We have compared our results with some observational data. Regarding the photometry, the density profiles across radial cuts in rings and spiral arms agree with the ones obtained from observations. The velocities along the ring also show that these are only a small perturbation of the circular velocity.

Acknowledgements

References

1. P.B. Eskridge, J.A. Frogel, R.W. Podge, A.C. Quillen, R.L. Davies, D.L. De-Poy, M.L. Houdashelt, L.E. Kuchinski, S.V. Ramírez, K. Sellgren, D.M. Terndrup, G.P. Tiede, *AJ*, **119**, 536 (2000)
2. D.M. Elmegreen, B.G. Elmegreen, *MNRAS*, **201**, 1021 (1982)
3. A. Sandage, J. Bedke, "The Carnegie Atlas of Galaxies", Carnegie Inst. Washington (1994)
4. B. Lindblad, *Stockholms Observatorium Ann.*, **Vol. 22**, No. 5 (1963)
5. A. Toomre, *ApJ*, **158**, 899 (1969)
6. P.O. Lindblad, *Stockholms Observatorium Ann.*, **Vol. 21**, No. 4 (1960)
7. A. Toomre, J. Toomre, *ApJ*, **178**, 623 (1972)
8. R.H. Sanders, J.M. Huntley, *ApJ*, **209**, 53 (1976)
9. A. Toomre, "The structure and evolution of normal galaxies", eds. S.M. Fall and D. Lynden-Ball, Proc. of the Advanced Study Institute, Cambridge, pp. 111-136 (1981)
10. E. Athanassoula, *Phys. Rep.*, **114**, 319 (1984)
11. M.P. Schwarz, *ApJ*, **247**, 77 (1981)
12. M.P. Schwarz, *MNRAS*, **209**, 93 (1984)
13. M.P. Schwarz, *MNRAS*, **212**, 677 (1985)
14. R. Buta, *ApJS*, **96**, 39 (1995)
15. E. Athanassoula, *MNRAS*, **259**, 328 (1992)
16. G. Kuzmin, *Astron. Zh.*, **33**, 27 (1956)
17. A. Toomre, *ApJS*, **138**, 385 (1963)
18. N.M. Ferrers, *Q.J. Pure Appl. Math.*, **14**, 1 (1877)
19. W. Dehnen, *AJ*, **119**, 800 (2000)
20. B. Barbanis, L. Woltjer, *ApJ*, **150**, 461 (1967)
21. M. Romero-Gómez, J.J. Masdemont, E. Athanassoula, C. García-Gómez, *A&A*, **453**, 39 (2006)

22. A. Lyapunov, *Ann. Math. Studies*, **17** (1949)
23. M. Romero-Gómez, E. Athanassoula, J.J. Masdemont, C. García-Gómez, *A& A*, **472**, 63 (2007)